Desalination and Water Treatment
www.deswater.com

doi: 10.5004/dwt.2023.30088

315 (2023) 32–39
December

In-situ construction of Bi_2S_3/BiOI heterojunctions with boosted photocatalytic activity

Chengxu Lai, Junbo Zhong*, Shengtian Huang, Minjiao Li

Key Laboratory of Green Catalysis of Higher Education Institutes of Sichuan, School of Chemistry and Environmental Engineering, Sichuan University of Science and Engineering, Zigong 643000, China, email: junbozhong@suse.edu.cn (J. Zhong)

Received 24 June 2023; Accepted 15 October 2023

ABSTRACT

In this demonstration, Bi_2S_3/BiOI composites were *in-situ* fabricated by a routine hydrothermal approach using KI, l-cysteine and $Bi(NO_3)_3{\cdot}5H_2O$ as raw materials. The Bi_2S_3/BiOI composites were studied by Brunauer–Emmett–Teller equation, X-ray diffraction, scanning electron microscopy, surface photovoltage spectroscopy, and electrochemical test. The observations confirm that the construction of Bi_2S_3/BiOI composites dramatically boosts the light response capacity, and separation of photoinduced carriers. Photocatalytic behaviors of the composites were investigated and compared with the reference BiOI by the disintegration of Rhodamine B. The outcomes firmly confirm that Bi_2S_3/BiOI heterostructures exhibit excellent photocatalytic performance and have promising application prospects in wastewater treatment.

Keywords: Photocatalysis; BiOI; Heterojunctions; Separation of carriers; Activity

1. Introduction

Serious environmental pollution caused by the random discharge of wastewater, exhaust gas into the environment has triggered considerable attention [1–3], the deteriorated environment significantly affects the survival and development of human beings and biospheres. To achieve sustainability of human society, it is crucial to purify the environment. Up to now, massive strategies have been applied to treat contaminants and create a comfortable environment for human society [4–6]. Among the various methods, photocatalytic technology has attracted considerable interest owing to its inherent advantages, such as low power consumption, safe, easy to operation, environmentally friendly and relative high efficiency [7–9]. Tremendous studies have shown that photocatalytic technology is one of the promising strategies to destruct pollutants [10–12]. To implement high-efficiency photocatalysis, fabrication and development of highly efficient photocatalysts is the core step. Amongst the massive photocatalysts, BiOI has drawn intense attention in light of its layered structure and strong visible light response ability [13–15]. However, BiOI suffers from low photocatalytic activity owing to the low separation rate of carriers [16–18]. To meet the practical application of BiOI, it is significant to elevate the photocatalytic activity of BiOI by ameliorating the separation of carriers. Extensive approaches have been used to boost the separation of photoinduced carriers, such as doping [19], construction of defects [14,20], morphology regulation [21], and building of heterojunctions [22,23], and so on. Among all these approaches, construction of heterostructures is deemed as one of the practical methods to boost the activity of BiOI [24–26]. Construction of BiOI-based heterojunctions demands another photocatalyst that can match the band structure of BiOI, thus an interfacial electric field will be established, facilitating the separation of photoinduced carriers and boosting the activity.

Amongst the various photocatalysts, Bi_2S_3 is an ideal candidate to couple with BiOI. Bi_2S_3 is a photocatalyst with narrow bandgap (~1.3 eV) and a layered structure [27,28], the unique features endow with Bi_2S_3 strong response to

* Corresponding author.

visible light and high photocatalytic activity. Naturally, Bi_2S_3 is widely employed to couple with other semiconductors to construct heterojunctions, largely ameliorating the photocatalytic ability of the heterostructures, for example, Bi_2S_3/Bi_5O_7I [28], Bi_2S_3@Ti_3C_2 [29], $Bi_2S_3/KTa_{0.75}Nb_{0.25}O_3$ [30], Bi_2S_3/SnS_2 [31] and so on.

Bi_2S_3/BiOI heterojunctions have been prepared by many researchers. Arumugam et al. [32] prepared 1D-Bi_2S_3@2D-GO/3D-BiOI ternary nanocomposite by a facile wet chemical method, the degradation efficiency of tetracycline is significantly enhanced on the 2%-Bi_2S_3@1%-GO/BiOI ternary nanocomposite. Cao et al. [33] fabricated Bi_2S_3/BiOI heterostructures through a facile and economical ion exchange method between BiOI and thioacetamide (CH_3CSNH_2), the optimal content of Bi_2S_3 is 4% with maximal photocatalytic degradation efficiency of 81.9% (5 h). Fang et al. [34] prepared BiOI/Bi_2S_3 heterojunctions by a soft chemical route using BiOI and thioacetamide. Wang et al. [35] BiOI/Bi_2S_3@ polydopamine nanosheets with thioacetamide, coupling BiOI with Bi_2S_3 can elevate the charge separation efficiency. The above studies firmly prove that the construction of Bi_2S_3/BiOI can strongly boost the performance of the composites. However, the construction of Bi_2S_3/BiOI heterostructures with strong interface interaction by a facile and wild approach is still a challenge. Closely interface interaction is prerequisite for the construction of heterojunctions, which will definitely affect the separation of photogenerated carriers and the stability of the composites.

In this paper, Bi_2S_3/BiOI composites were *in-situ* fabricated by a hydrothermal method using l-cysteine and KI. Under a hydrothermal environment, Bi_2S_3/BiOI heterojunctions will be *in-situ* formed with strong interface interaction. The Bi_2S_3/BiOI heterojunctions built will be carefully studied by serval methods, photocatalytic activities of the samples were evaluated by decontamination of Rhodamine B (RhB). The results show that Bi_2S_3/BiOI heterojunctions demonstrate higher activity than the reference BiOI, and the composites exhibit excellent stability. Construction of Bi_2S_3/BiOI heterojunctions using l-cysteine is a reliable strategy to boost the activity of BiOI, this method can be applied to prepare other highly efficiency photocatalysts.

2. Experimental sections

Detailed information was provided in the Supporting Information.

3. Results and discussion

3.1. Characterization

The specific surface area of the samples is demonstrated in Table 1. Clearly, the specific surface area of the samples gradually increases as the loading of l-cysteine, which firmly shows that adding l-cysteine into the preparation system of BiOI dramatically affects the crystal growth of BiOI, resulting in relatively high specific surface area. Commonly, a high specific surface area is favorable for photocatalytic activity [36]. However, in light of the photocatalytic activity, specific surface area is not the leading factor that determines the photocatalytic performance in this case.

Table 1
Specific surface area of the samples

Sample	S_{BET} (m^2/g)
BiOI	1.6
5%	2.6
10%	1.5
15%	2.1
20%	2.4

X-ray diffraction (XRD) information of the samples is revealed in Fig. 1. As illustrated in Fig. 1A, evidently, the 0% sample corresponds to the BiOI (PDF# 10-0445), no other peaks were detected, indicating high purity of the samples. Compared to the reference BiOI, the diffraction peaks for the (001) plane of the composites become stronger, which strongly affirms that Bi_2S_3 influences the crystal growth of BiOI. From XRD patterns of the composites, no diffraction peaks for Bi_2S_3 were detected, which can be attributed to the low content of Bi_2S_3 or high dispersion on the surface of BiOI. To confirm the existence of Bi_2S_3 in the composites, the XRD profiles of the sample prepared with high molar ratio of S/Bi (3/1) is shown in Fig. 1B, compared with the standard diffraction peaks of Bi_2S_3 (PDF 75-1306), the sample with 3/1 molar ratio of S/Bi exhibits typical diffraction peaks of Bi_2S_3, which indicates that Bi_2S_3 can be availably obtained by a hydrothermal method using $Bi(NO_3)_3{\cdot}5H_2O$ and l-cysteine, thus Bi_2S_3 exists in the composites. Fig. 1C shows the enlarged vision of the diffraction peaks of the (001) plane of the samples, it is evident the diffraction peaks of the (001) plane of the composites shift toward a lower angle, which substantially proves a strong interaction exists between Bi_2S_3 and BiOI, which is beneficial to construct Bi_2S_3/BiOI heterojunctions. Moreover, according to $2d\sin\theta = n\lambda$, the interplanar spacing between the (001) plane increases, inducing by the coupling Bi_2S_3 with BiOI. All the above results firmly show that Bi_2S_3/BiOI heterojunctions have been successfully *in-situ* constructed.

Morphology of the photocatalyst plays an important role in affecting the performance of photocatalysts, therefore, it is crucial to investigate the change in morphology of the photocatalyst after integrating Bi_2S_3 with BiOI. Illustrated in Fig. 2A and B, both the reference BiOI and 15% sample display a lump-like appearance, which suggests that low loading of Bi_2S_3 cannot effectively change the shape of the photocatalyst. However, the 15% sample exhibits a smaller particle size than the reference BiOI, small particle size can elevate the specific surface area, according well with the measurement results of S_{BET}. Fig. 2C displays energy-dispersive X-ray spectroscopy (EDS) pattern of the 20% sample, apparently, O, S and Bi were observed. Combined with EDS and XRD results, it is obvious that Bi_2S_3/BiOI heterojunctions with strong interaction were *in-situ* built.

Optical properties of the photocatalysts were studied, and the results are revealed in Fig. 3A. Clearly, the absorption edge of the photocatalyst appears to red-shift as the loading of Bi_2S_3 elevates owing to the narrow bandgap of Bi_2S_3. Enhanced light absorption capacity is conducive to photocatalytic activity. In the $\alpha h\nu = A(h\nu - E_g)^n$ formula, where

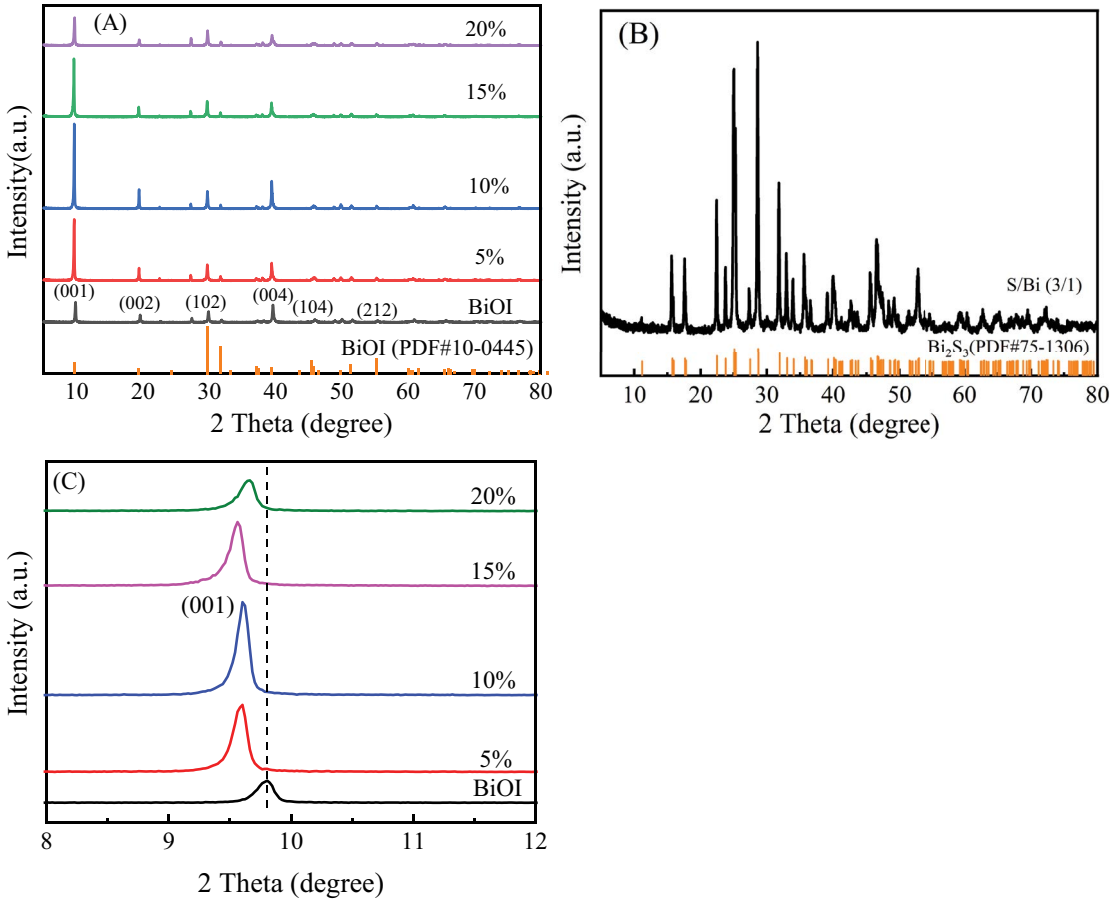

Fig. 1. (A) X-ray diffraction patterns of the samples, (B) X-ray diffraction profiles of the sample prepared with 3/1 molar ratio of S/Bi, and (C) enlarged vision of the diffraction peaks of the (001) plane of the photocatalysts.

h, *v*, and *A* stand for the absorption coefficient, Planck coefficient, optical frequency and constants, respectively. In the equation for indirect semiconductors, *n* is equal to 2 [37,38]. Bandgaps of all the samples can be calculated according to $\alpha h\nu = A(h\nu - E_g)^2$ [39], as shown in Fig. 3B, the bandgap of BiOI and the 15% sample is 1.29 and 1.38 eV, separately. The narrowed bandgap of the 15% sample is allocated to the existence of Bi_2S_3 in the composites and the bandgap of Bi_2S_3 is narrower than that of BiOI. Generally, a narrow bandgap is beneficial to solar light-driven photocatalytic activity.

During the photocatalytic process, so many factors can determine the photocatalytic activity, among all the factors, the separation of the photoinduced carriers performs a leading role in determining the photocatalytic activity of the photocatalyst, consequently, it is absolutely necessary to study the separation behaviors of photogenerated carriers. Surface photovoltage spectroscopy (SPS) responses of the samples induced under light irradiation are shown in Fig. 4A, it is evident that all the photocatalysts display detectable SPS from 300 to 600 nm, which can be assigned to the jump of electrons from the valence band to the conduction band, which generates the change in the surface potential barrier, displaying SPS signals. All the Bi_2S_3/BiOI composites exhibit stronger SPS signals than the reference BiOI, more importantly, the Bi_2S_3/BiOI heterojunctions possess obvious SPS response from 600 to 700 nm. Clearly, the enhanced SPS strength and range of SPS is definitely allocated to the existence of Bi_2S_3 in the composites. The SPS signal intensity of the sample gradually elevates as the loading of Bi_2S_3 boosts, among all the photocatalysts, the 15% photocatalyst holds the strongest SPS response. However, SPS response begins to drop as the amount of Bi_2S_3 further increases. Excessive Bi_2S_3 on the surface of BiOI will inhibit the light from penetrating the interface of Bi_2S_3/BiOI, holding low SPS signals. According to the measurement principle [40], a strong SPS response designates a high separation rate of photoexcited carriers. Generally, a high separation rate of photoactivated carriers is favorable for the photocatalytic activity, thereby, it is anticipated that the 15% sample will possess the highest activity. To further investigate the separation property of carriers, the photocurrent generated by the samples under simulated sunlight irradiation was measured. As revealed in Fig. 4B, photocurrent intensity of the 15% sample is higher than that of the reference BiOI, which agrees well with SPS results. Presented in Fig. 4C, in comparison with the reference BiOI, the 15% photocatalyst holds obviously smaller impedance, which implies that the 15% photocatalyst has lower migration resistance for photoinduced electrons than the reference BiOI, which is advantageous to the separation of photoexcited carriers, according well with photocatalytic activity.

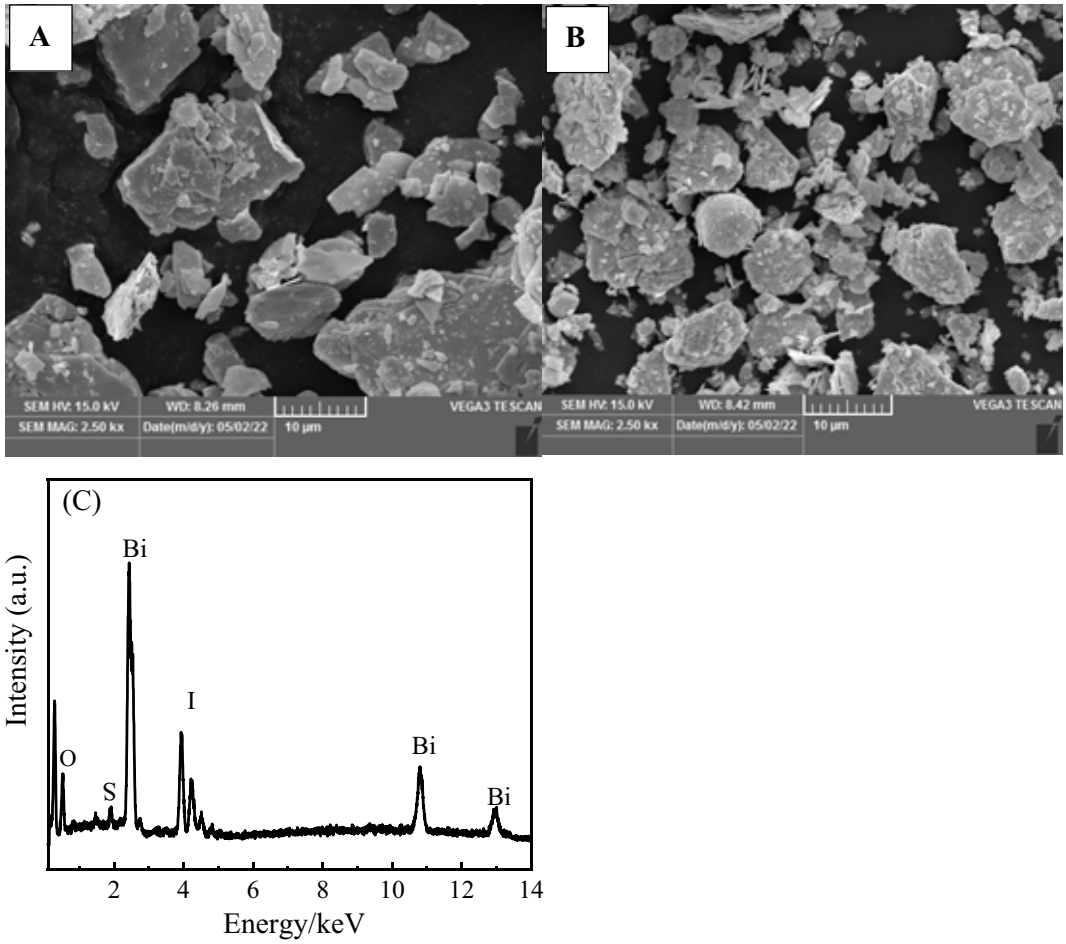

Fig. 2. Scanning electron microscopy images of BiOI (A), 15% sample (B), energy-dispersive X-ray spectroscopy patterns of the 20% sample (C).

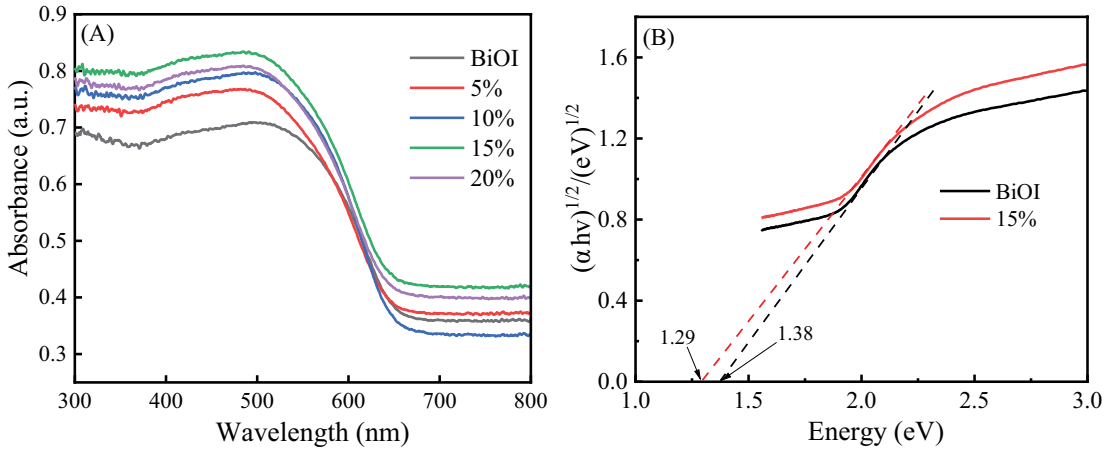

Fig. 3. (A) Optical properties of the samples and (B) bandgap of BiOI and 15% sample.

3.2. Photocatalytic activity measurement

Photocatalytic performance of the photocatalysts was investigated by destruction of RhB under simulated sunlight illumination. As shown in Fig. 5A, the adsorption–desorption equilibrium of Rhodamine B over the sample can be quickly established, and Rhodamine B can be effectively destructed over the photocatalysts, the decay of RhB over the sample can be mainly allocated to photocatalysis. Amongst the samples, the 15% sample has the highest activity. The decontamination of RhB on the photocatalyst can

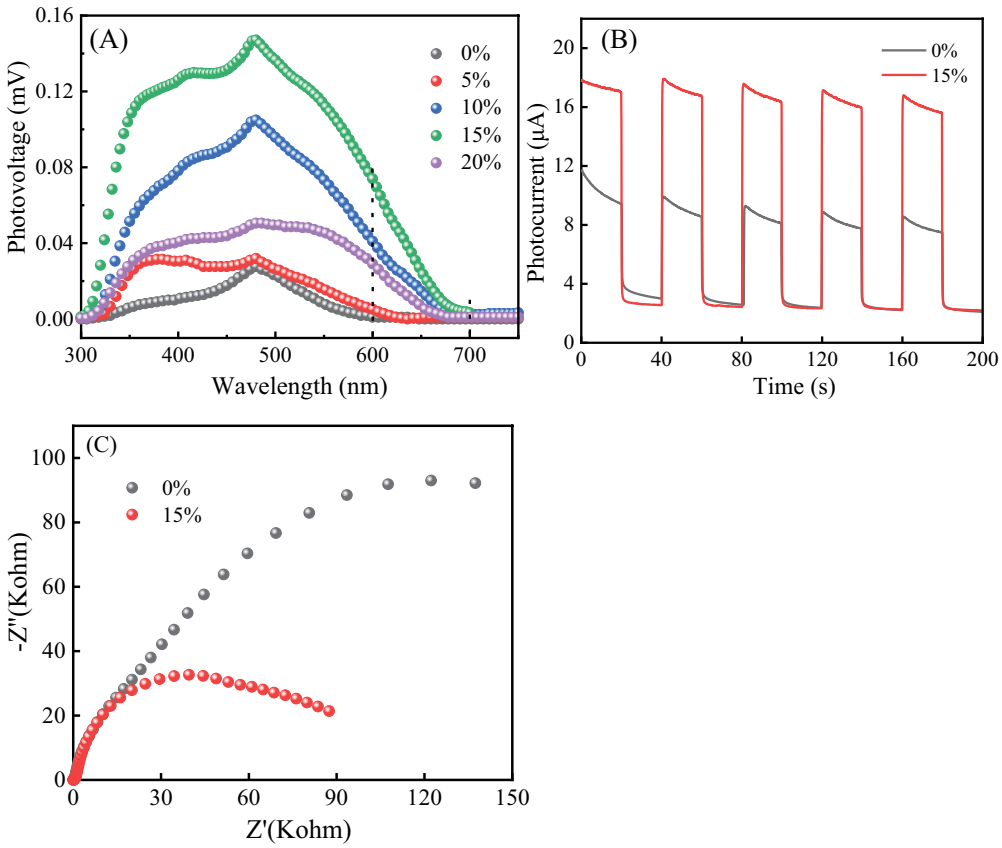

Fig. 4. (A) Surface photovoltage spectroscopy signals of BiOI and the Bi_2S_3/BiOI samples, (B) photocurrent responses, and (C) IS spectra of BiOI and the 15% sample.

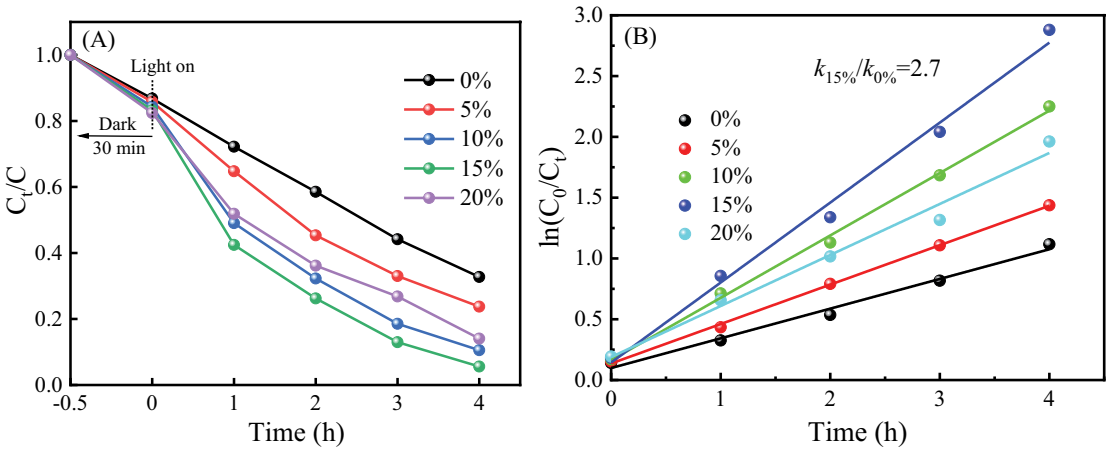

Fig. 5. (A) Photocatalytic decay of Rhodamine B and (B) relevant rate constant of Rhodamine B on all the samples.

be described by a first-order kinetic, namely, $\ln(C_0/C_t) = kt$, where C_0 and C_t is the concentration of Rhodamine B before irradiation and the concentration of Rhodamine B at the moment after light irradiation, respectively, while k is the degradation rate constant of RhB. High k indicates high photocatalytic activity. As demonstrated in Fig. 5B, all the Bi_2S_3/BiOI samples display higher activity than the reference BiOI, and the 15% photocatalyst holds the highest activity, the activity of the 15% sample is 2.7 times of that of the blank BiOI. Interestingly, the trend in photocatalytic activity fits well with the results of the separation of photoinduced carriers, confirming that the separation of photoinduced carriers plays a leading role in influencing the activity of photocatalysts. However, excessive Bi_2S_3 loading on the BiOI surface interferes with photoexcitation, thus activity of the 20% catalyst is lower than that of the 15% catalyst. This result is consistent with the previous XRD, UV and SPS test results. From the above results, it is apparent that coupling

Bi_2S_3 with BiOI by a facile hydrothermal approach is a reliable strategy to boost the activity of BiOI.

As shown in Fig. 6A, the degradation efficiency of RhB on the catalyst varies at different pH, and the degradation efficiency of Rhodamine B is highest at pH = 7.0. The degradation efficiency of Rhodamine B is inhibited at both pH = 2 and pH = 12. Fig. 6B shows that the degradation efficiency is partially inhibited when the dosage of catalyst due to the scattering effect of particles. As demonstrated in Fig. 6C, the highest degradation rate is observed when the concentration of RhB is 10 mg/L, and the degradation efficiency is suppressed by gradually increasing concentration

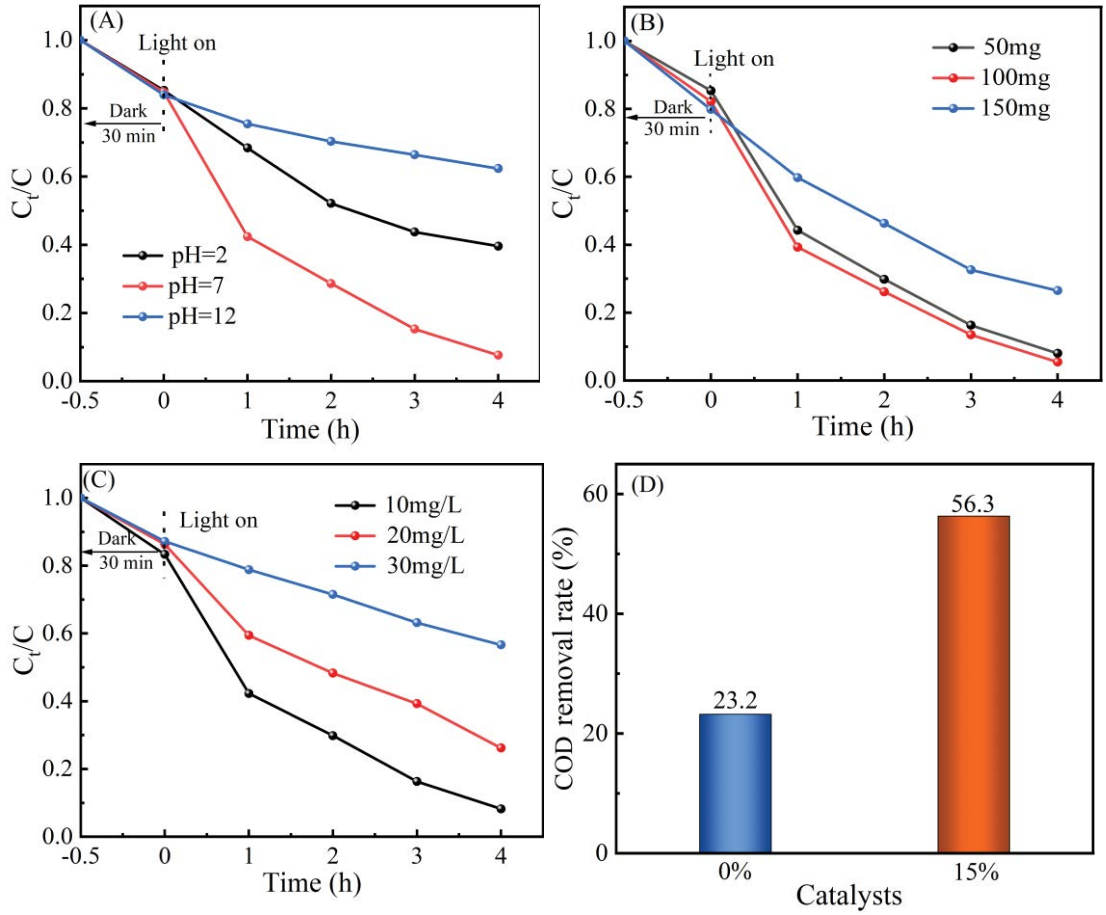

Fig. 6. (A) Degradation rates of catalyst at different pH conditions, (B) degradation rates of catalyst at different dye concentrations, (C) degradation rates at different catalyst dosages, and (D) effect of different catalysts on chemical oxygen demand removal (The contaminant is Rhodamine B and the light source is a xenon lamp).

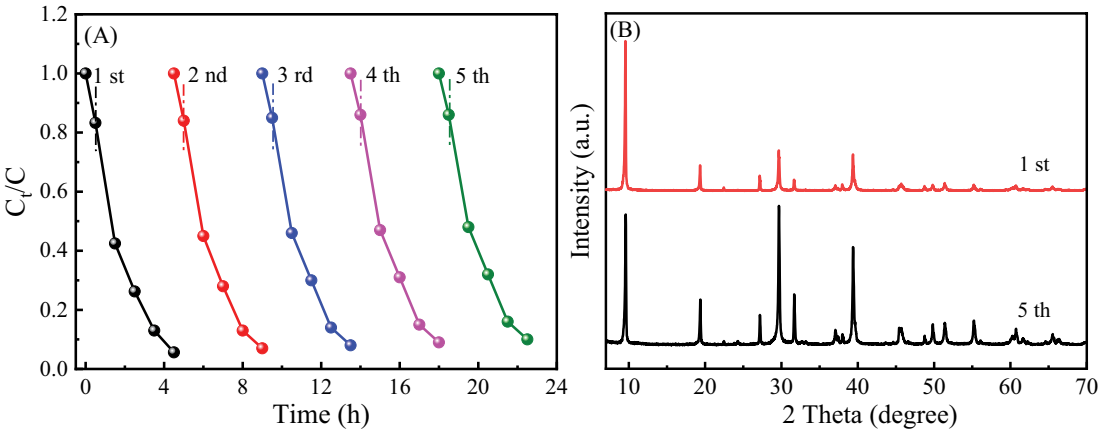

Fig. 7. Cycle experiment (A) and X-ray diffraction patterns photocatalytic cycles (B) of the 15% sample.

of Rhodamine B. In Fig. 6D, after irradiation for 180 min, the chemical oxygen demand (COD) removal of Rhodamine B on the 0% and 15% catalysts is 23.2% and 56.3%, respectively, which indicates that activity of the composite catalysts is enhanced and the COD removal rate increases significantly.

Stability of the photocatalyst is an important factor which influences the practical application of photocatalyst. Cycle experiments for the 15% sample were performed. As demonstrated in Fig. 7A, after five cycles, no obvious drop-in photocatalytic activity was observed, firmly affirming the stability of the samples originated from strong interaction between Bi_2S_3 and BiOI. XRD patterns of the 15% sample before and after the photocatalytic cycle are illustrated in Fig. 7B, no new peaks appear. The results strongly support the stability of the sample, and the photocatalysts have promising applications in wastewater purification.

4. Conclusion

In this work, Bi_2S_3/BiOI heterojunctions were *in-situ* constructed by a facile hydrothermal method with the assistance of l-cysteine. Fabrication of Bi_2S_3/BiOI heterojunctions can be solidly proven by XRD and EDS. Integration of Bi_2S_3 with BiOI promotes the specific surface area, on the whole, widens the light response range, and boosts the separation of photoinduced carriers. All the Bi_2S_3/BiOI heterostructures show higher photocatalytic activity than BiOI, when the molar ratio of S/Bi is 15%, the sample displays the highest activity for detoxification of RhB, which is 2.7 times of that of BiOI. Moreover, the composites have excellent stability. This work offers a significant strategy to *in-situ* constructing heterostructures containing Bi_2S_3.

Data availability statement

The authors confirm that the data supporting the findings of this study are available within the article.

Acknowledgment

The authors thank Sichuan University of Science and Engineering (No.2021RC26) and city of Zigong (2020YGJC27) for financial support.

References

[1] H. Liao, Y. Ran, J. Zhong, J. Li, M. Li, H. Yang, Panax notoginseng powder-assisted preparation of carbon-quantum-dots/BiOCl with enriched oxygen vacancies and boosted photocatalytic performance, Environ. Res., 215 (2022) 114366, doi: 10.1016/j.envres.2022.114366.

[2] A. Dubsok, P. Khamdahsag, S. Kittipongvises, Life cycle environmental impact assessment of cyanate removal in mine tailings wastewater by nano-TiO_2/$FeCl_3$ photocatalysis, J. Cleaner Prod., 366 (2022) 132928, doi: 10.1016/j.jclepro.2022.132928.

[3] W. Ji, X. Wang, T. Ding, S. Chakir, Y. Xu, X. Huang, H. Wang, Electrospinning preparation of nylon-6@UiO-66-NH_2 fiber membrane for selective adsorption enhanced photocatalysis reduction of Cr(VI) in water, Chem. Eng. J., 451 (2023) 138973, doi: 10.1016/j.cej.2022.138973.

[4] K. Liu, J. Chen, F. Sun, Y. Liu, M. Tang, Y. Yang, Historical development and prospect of intimately coupling photocatalysis and biological technology for pollutant treatment in sewage: a review, Sci. Total Environ., 835 (2022) 155482, doi: 10.1016/j.scitotenv.2022.155482.

[5] L.N. Warr, A. Friese, F. Schwarz, F. Schauer, R.J. Portier, L.M. Basirico, G.M. Olson, Experimental study of clay-hydrocarbon interactions relevant to the biodegradation of the deepwater horizon oil from the Gulf of Mexico, Chemosphere, 162 (2016) 208–221.

[6] F. Liu, Z. Zhou, Y. Tu, J. Chen, F. Zhang, S. Tian, Z. Ren, Preparation of green sodium alginate adsorption membrane and its high adsorption performance for fluoroquinolones antibiotics, J. Water Process Eng., 49 (2022) 103124, doi: 10.1016/j.jwpe.2022.103124.

[7] H. Li, T. Zhang, X. Tang, J. Zhong, J. Li, Z. Du, Y. Dan, Effectively destruction of Rhodamine B and perfluorooctanoic acid over BiOCl with boosted separation ability of carriers benefited from tunable oxygen vacancies, Colloid. Surf., A, 649 (2022) 129470, doi: 10.1016/j.colsurfa.2022.129470.

[8] X. Jin, X. Tang, H. Li, X. Tang, J. Li, J. Zhong, S. Zhang, D. Ma, Visible-light driven efficient elimination of organic hazardous and Cr(VI) over BiOCl modified by Chinese Baijiu distillers' grain-based biochar, J. Ind. Eng. Chem., 107 (2022) 472–482.

[9] Y. He, Y. Chen, S. Lei, J. Zhong, M. Li, Rich oxygen vacancies facilitated visible light-driven removal of phenol and Cr(VI) over Bi_2WO_6 decorated by sorghum straw carbon, Colloids Surf., A, 641 (2022) 128534, doi: 10.1016/j.colsurfa.2022.128534.

[10] H. Liao, J. Zhong, J. Li, Tunable oxygen vacancies facilitated removal of PFOA and RhB over BiOCl prepared with alcohol ether sulphate, Appl. Surf. Sci., 590 (2022) 152891, doi: 10.1016/j.apsusc.2022.152891.

[11] F. Liu, H. Cao, L. Xu, H. Fu, S. Sun, Z. Xiao, C. Sun, X. Long, Y. Xia, S. Wang, Design and preparation of highly active TiO_2 photocatalysts by modulating their band structure, J. Colloid Interface Sci., 629 (2023) 336–344.

[12] J. Ke, Y. Ge, Q. Yang, Y. Liu, P.L. Show, R. Guo, J. Che, Degradation of sulfamethazine using sludge-derived photocatalysts from dyeing industry and livestock farm: preparation and mechanism, J. Hazard. Mater., 440 (2022) 129837, doi: 10.1016/j.jhazmat.2022.129837.

[13] Y. Chen, J. Huang, J. Zhong, M. Li, Z. Li, C. Yang, Enhanced photocatalytic performance of TiO_2/BiOI heterojunctions benefited from effective separation of photogenerated carriers, Chem. Phys. Lett., 780 (2021) 138966, doi: 10.1016/j.cplett.2021.138966.

[14] H. Liao, Z. Li, L. Luo, J. Zhong, J. Li, Water hyacinth powder-assisted preparation of defects-rich and flower-like BiOI/Bi_5O_7I heterojunctions with excellent visible light photocatalytic activity, Surf. Interfaces, 27 (2021) 101470, doi: 10.1016/j.surfin.2021.101470.

[15] Y. Wang, X. Liu, Q. Chen, T.C. Zhang, L. Ouyang, S. Yuan, Simultaneous photocatalytic oxidation and adsorption for efficient As(III) removal by magnetic BiOI/γ-Fe_2O_3 core–shell nanoparticles, Mater. Today Chem., 24 (2022) 100823, doi: 10.1016/j.mtchem.2022.100823.

[16] T. Wang, C. Zhao, L. Meng, Y. Li, H. Chu, F. Wang, Y. Tao, W. Liu, C.C. Wang, *In-situ*-construction of BiOI/UiO-66 heterostructure via nanoplate-on-octahedron: a novel *p-n* heterojunction photocatalyst for efficient sulfadiazine elimination, Chem. Eng. J., 451 (2023) 138624, doi: 10.1016/j.cej.2022.138624.

[17] K. Li, Y. Zhang, X. Zhang, B.J. Ni, Y. Wei, B. Xu, D. Hao, A readily synthesized bismuth oxyiodide/attapulgite for the photodegradation of tetracycline under visible light irradiation, CrystEngComm, 24 (2022) 3064–3073.

[18] J. Cai, Y. Xiao, Y. Tursun, A. Abulizi, Z-type heterojunction of Cu_2O-modified layered BiOI composites with superior photocatalytic performance for CO_2 reduction, Mater. Sci. Semicond. Process., 149 (2022) 106891, doi: 10.1016/j.mssp.2022.106891.

[19] J. Xiong, H.Y. Zeng, S. Xu, J.F. Peng, F.Y. Liu, L.H. Wang, Enhancing the intrinsic properties of flower-like BiOI by S-doping toward excellent photocatalytic performances, J. Mater. Sci. Technol., 118 (2022) 181–189.

[20] C. Hu, H.X. Huang, Y.F. Lin, K.L. Tung, T.H. Chen, L. Lo, Heterostructural design of I-deficient BiOI for photocatalytic decoloration and catalytic CO_2 conversion, Catal. Sci. Technol., 9 (2019) 3800–3811.

[21] L. Zhong, C. Wang, X. Cui, Use of mesoporous BiOI microspheres for sonocatalytic degradation of tetracycline

hydrochloride, Ecotoxicol. Environ. Saf., 237 (2022) 113547, doi: 10.1016/j.ecoenv.2022.113547.
[22] C. Yin, Y. Liu, X. Lv, S. Lv, H. Cheng, X. Kang, X. Li, Carbon dots as heterojunction transport mediators effectively enhance BiOI/g-C_3N_4 synergistic persulfate degradation of antibiotics, Appl. Surf. Sci., 601 (2022) 154249, doi: 10.1016/j.apsusc.2022.154249.
[23] J. Jiang, Y. Song, X. Wang, T. Li, M. Li, Y. Lin, T. Xie, S. Dong, Enhancing aqueous pollutant photodegradation via a Fermi level matched Z-scheme BiOI/Pt/g-C_3N_4 photocatalyst: unobstructed photogenerated charge behavior and degradation pathway exploration, Catal. Sci. Technol., 10 (2020) 3324–3333.
[24] Q. Li, S. Gao, J. Hu, H. Wang, Z. Wu, Superior NO_x photocatalytic removal over hybrid hierarchical Bi/BiOI with high non-NO_2 selectivity: synergistic effect of oxygen vacancies and bismuth nanoparticles, Catal. Sci. Technol., 8 (2018) 5270–5279.
[25] C.L. Hsu, Y.J. Li, H.J. Jian, S.G. Harroun, S.C. Wei, R. Ravindranath, J.Y. Lai, C.C. Huang, H.T. Chang, Green synthesis of catalytic gold/bismuth oxyiodide nanocomposites with oxygen vacancies for treatment of bacterial infections, Nanoscale, 10 (2018) 11808–11819.
[26] Y. Du, R. Ma, L. Wang, J. Qian, Q. Wang, 2D/1D BiOI/g-C_3N_4 nanotubes heterostructure for photoelectrochemical overall water splitting, Sci. Total Environ., 838 (2022) 156166, doi: 10.1016/j.scitotenv.2022.156166.
[27] Y. Liu, M. Li, Y. Zheng, H. Lin, Z. Wang, W. Xin, C. Wang, F. Du, Boosting potassium-storage performance via the functional design of a heterostructured Bi_2S_3@RGO composite, Nanoscale, 12 (2020) 24394–24402.
[28] P. Ju, L. Hao, Y. Zhang, J. Sun, K. Dou, Z. Lu, D. Liao, X. Zhai, C. Sun, *In-situ* topotactic construction of novel rod-like Bi_2S_3/Bi_5O_7I *p-n* heterojunctions with highly enhanced photocatalytic activities, J. Mater. Sci. Technol., 135 (2023) 126–141.
[29] X. Wang, H. Zhang, W. Wang, G. Zhang, X. Chu, J. Cao, Synthesis of 1D/2D Bi_2S_3@Ti_3C_2 heterojunction with superior photocatalytic removal ability of tetracycline hydrochloride, Mater. Lett., 326 (2022) 132907, doi: 10.1016/j.matlet.2022.132907.
[30] L. Chen, X. Dai, X. Li, J. Wang, H. Chen, X. Hu, H. Lin, Y. He, Y. Wu, M. Fan, A novel Bi_2S_3/$KTa_{0.75}Nb_{0.25}O_3$ nanocomposite with high efficiency for photocatalytic and piezocatalytic N_2 fixation, J. Mater. Chem. A, 9 (2021) 13344–13354.
[31] S. Paul, D. Barman, C. Chowdhury, P.K. Girib, S.K. De, 3D/2D Bi_2S_3/SnS_2 heterostructures: superior charge separation and enhanced solar light-driven photocatalytic performance, CrystEngComm, 23 (2021) 2276–2288.
[32] M. Arumugam, S.J. Lee, T. Begildayeva, S.S. Naik, Y. Yu, H. Lee, J. Theerthagiri, M.Y. Choi, Enhanced photocatalytic activity at multidimensional interface of 1D-Bi_2S_3@2D-GO/3D-BiOI ternary nanocomposites for tetracycline degradation under visible-light, J. Hazard. Mater., 404 (2021) 123868, doi: 10.1016/j.jhazmat.2020.123868.
[33] J. Cao, B. Xu, H. Lin, B. Luo, S. Chen, Novel heterostructured Bi_2S_3/BiOI photocatalyst: facile preparation, characterization and visible light photocatalytic performance, Dalton Trans., 41 (2012) 11482–11490.
[34] M. Fang, H. Jia, W. He, Y. Lei, L. Zhang, Z. Zheng, Construction of flexible photoelectrochemical solar cells based on ordered nanostructural BiOI/Bi_2S_3 heterojunction films, Phys. Chem. Chem. Phys., 17 (2015) 13531–13538.
[35] Z. Wang, L. Wang, S. Liu, M. Zhang, Y. Li, L. Rong, Y. Liu, H. Zhang, Z-scheme heterostructures for glucose oxidase-sensitized radiocatalysis and starvation therapy of tumors, Nanoscale, 14 (2022) 2186–2198.
[36] H. Liao, J. Zhong, J. Li, Tunable oxygen vacancies facilitated removal of PFOA and RhB over BiOCl prepared with alcohol ether sulphate, Appl. Surf. Sci., 590 (2022) 152891, doi: 10.1016/j.apsusc.2022.152891.
[37] S.K. Suram, P.F. Newhouse, J.M. Gregoire, High throughput light absorber discovery, part 1: an algorithm for automated Tauc analysis, ACS Comb. Sci., 18 (2016) 673–681.
[38] J. Yi, R. Xie, R. Liu, M. Li, H. Zeng, Q. Chen, L. Cai, N. Li, C. Yu, Z. Liu, D. Li, Hollow BiOI/Bi_5O_7I hierarchical microsphere with S-scheme heterostructure for efficiently removal of tetracycline hydrochloride, J. Water Process Eng., 53 (2023) 103798, doi: 10.1016/j.jwpe.2023.103798.
[39] Y. He, Y. Chen, S. Lei, J. Zhong, M. Li, Rich oxygen vacancies facilitated visible light-driven removal of phenol and Cr(VI) over Bi_2WO_6 decorated by sorghum straw carbon, Colloids Surf., A, 641 (2022) 128534, doi: 10.1016/j.colsurfa.2022.128534.
[40] L. Kronik, Y. Shapira, Surface photovoltage phenomena: theory, experiment and application, Surf. Sci. Rep., 254 (1999) 1–205.

Supporting information

1. Experimental sections

All the chemicals are analytical reagent and were obtained from Chengdu Kelong Chemicals Co., Ltd., (Chengdu, China). 4.1 g $Bi(NO_3)_3{\cdot}5H_2O$ was dissolved in 40 mL glacial acetic acid, forming solution A. 1.4 g KI and desired l-cysteine were dissolved in 20 mL deionized water, obtaining solution B, the molar ratio of S/Bi is 0%, 5%, 10%, 15%, and 20%, respectively. Under intense agitation, solution B was slowly dropped into solution A by a constant flow pump, and then the suspension system was continuously stirred for 1 h. Afterward, the suspension was transferred into a 100 mL PTFE lined autoclave and kept at 180°C for 24 h. After the autoclave cooling down to room temperature, the samples were acquired by filtering, rinsing with deionized water, and ethanol for many times. The samples were obtained by drying at 80°C overnight. The sample fabricated with different molar ratios of S/Bi was designed as 0% (BiOI), 5%, 10%, 15%, and 20%, respectively.

Specific surface area of the sample was determined on an SSA-4200 tester. The crystal information was attained on an D2 PHASER X-ray diffractometer (Bruker). Morphologies of the samples were observed on a VEGA3 SBU scanning electron microscopy with energy-dispersive X-ray spectroscopy. The optical properties were studied on a UH4150 UV-Vis spectrophotometer using $BaSO_4$ as the reference. Separation behavior of the carriers was measured on a self-assembled surface photovoltage spectroscopy and a CHI660E electrochemical workstation with a 500 W xenon lamp.

Photocatalytic performance of the catalysts was evaluated by destruction of Rhodamine B (RhB) under a 500 W xenon lamp (simulated solar light). The initial mass concentration of Rhodamine B solution was 10 mg/L, the dosage of photocatalyst was 1 g/L. Before the photocatalytic reaction, the suspension system was stirred for 30 min in dark to establish adsorption–desorption equilibrium. At regular timespan, intervals, 5 mL the turbid solution was sampled, after centrifuging, the residual RhB was analyzed on a TU-1950 UV-Vis spectrophotometer. Total organic carbon (TOC) of RhB solution was tested using a Vario TOC analyzer.